SPE 166307

Fracture Characterization in Unconventional Reservoirs using Active and Passive Seismic Data with Uncertainty Analysis through Geostatistical Simulation

D. Maity, and F. Aminzadeh, SPE, University of Southern California

Abstract

This study discusses a new workflow for fracture characterization and modeling using geophysical (microseismic and 3D surface seismic) data along with independent reservoir information (such as well logs). The framework is ideally suited for unconventional environments such as shale and tight reservoirs where modern technologies such as the use of hydraulic fracturing and passive seismic monitoring allow application of the proposed workflow.

The workflow involves generating geomechanical property estimates (including stress and weakness estimates) as derived from passive seismic data analysis and relevant seismic attributes derived from 3D seismic data combined using ANN based reservoir property modeling framework. The training information for the networks is generated based on a-priori information through image logs. Resolution of passive seismic derived velocity models is improved by using sequential Gaussian co-simulation by combining low resolution velocity maps high resolution seismic impedance data for phase velocity estimation. Uncertainty estimates are quantified by adequate number of realizations and associated probability density functions for fracture properties within study volume.

In this paper, different properties estimated through ANN modeling have been shared. New fracture identifier (FZI) properties have been defined and the models have been used to characterize fracture zones and major discontinuities for a representative unconventional reservoir (geothermal setting) used in our study. We also share uncertainty estimates for the identified fracture zones for improved characterization. Finally fracture property estimates for the study area (derived using FZI and other properties) have been generated for future reservoir simulation studies.

The proposed method allows for improved understanding of shale and other unconventional reservoirs through fracture mapping and provides a workflow for improved volumetrics of the reservoir by making use of identified properties for fracture modeling. This work validates the potential for using relatively low resolution passive seismic data for improved reservoir characterization using Geostatistical tools. It also provides a valuable framework for pseudo 4D characterization where a single 3D seismic survey can be used as the basis to characterize the reservoir in a time lapse fashion using new information collected in time through passive seismic arrays as well as new well logs being obtained within the area of interest.

Introduction

Use of geophysical tools for reservoir characterization and monitoring is fairly well understood and has been used extensively in recent years. Passive seismic monitoring has found applications in development of unconventional reservoirs such as geothermal systems involving injection and production of hot water or steam from the reservoir, tight gas and oil systems which require hydraulic fracturing and finally monitoring of injection wells (waste water, CO_2, etc.) among others. In the field of conventional seismic, techniques such as multi-attribute analysis and integrated analysis techniques are being used extensively for reservoir characterization. While conventional seismic data is rarely available for small unconventional reservoir developments, the use of microseismic data is limited to better understanding of the fracturing process including diagnosis and volumetrics but is seldom used

as a tool for reservoir property prediction. In our study, we have used seismic as well as microseismic data along with well logs to better predict the reservoir properties and understand the fractures within the study volume. This workflow involves simultaneous use of MEQ and Seismic data as well as mapped log derived properties as outlined in **Figure 1**. An ANN algorithm is used for fracture zone identification and characterization providing indication of zones with presence of open fractures. While this paper does not deal with actual modeling of fracture properties, it provides some of the necessary information for required fracture properties which in turn can be used as inputs for modeling workflows. Our aim is to demonstrate the potential for this workflow for small unconventional developments to improve understanding of the reservoir behavior with time and to optimize overall productivity from the reservoir over its development cycle.

The area of study is a shallow geothermal system within a complex sedimentary basin and an active geologic setting (Gulf of California Rift Zone). The study area has reasonably good well control with multiple production/ injection wells and associated well logs. A passive seismic array is used to continuously monitor the operations of the field. The acquisition array for the data used in this study includes 5 recording sensors placed in shallow boreholes, each recording 3 component continuous data. A single 3D field-wide seismic survey was conducted and the processed data was used in our attribute analysis workflow. Well logs were independently interpreted and evaluated properties (such as V_{sh} and ϕ) were mapped for the entire study volume using an ANN based attribute mapping scheme. Finally, crustal models were obtained from SCEC for local velocity field estimates as the available seismic data was made available without any velocity information.

Microseismic data analysis

A simple energy ratio based autopicker is used for preliminary detection of events. The triggered data is run through an advanced ANN based autopicking workflow (Aminzadeh et al. 2011) and the final picks obtained are used to detect phase arrivals for use with inversion algorithms for both location and velocity. Due to the nature of the data as well as limitations with the monitoring array design, only ~6% of the detected events are used in further analysis. **Figure 2** shows the final selected event epicenters along with the study area of interest plotted together indicating the potential noise and bias issues. The primary selection of detected events to be used in inversion is based on pick quality estimates. HypoDD (Waldhauser 2001) is used to obtain hypocentral locations using the event arrival times based on generated phase data as well as the baseline crustal models. Further pruning of events is done based on failure of inversion algorithm to properly resolve events based on iterative HypoDD runs. The final "selected" events are then used to generate improved velocity models by using SimulPS inversion algorithm (Thurber 1993). SimulPS uses phase information along with preliminary velocity estimates and progressively iterates over all of the phase data available to provide final hypocentral and velocity estimates. The final velocity models obtained are used as a baseline estimate for the area of interest. **Figure 3** shows sample V_P and V_S maps estimated at reference depth (0.5 km) confined within the study area alone.

3D seismic & well log analysis

Seismic attribute analysis is carried out to first identify major discontinuity features and other artifacts. These include Laplacian edge enhancement filter, curvature and similarity features, dip, variance and other attributes. Laplacian (edge enhancement methods based on dip steered 2nd order spatial derivatives (Jahne 1993)) and Amplitude variance as an edge preserving method (Bakker et al. 1999) are used for baseline discontinuity mapping for our study. **Figure 4** shows some of the mapped properties at the reference depth (0.5 km). Rock properties (such as ϕ, ρ) are estimated using ANN rock property prediction workflow using sample training and validation data from processed well logs and training attributes selected based on observed correlation between log properties and attributes. Relative acoustic impedance (Lancaster 2000) is used as a proxy for structural features in the subsurface and is used to improve the resolution of both the V_P and V_S models using COSGSIM algorithm.

Due to lack of available velocity models from seismic data processing and lack of depth migrated seismic volumes, a rudimentary time to depth conversion workflow is followed where well logs are used to obtain seismic to well ties. Due to the absence of sonic logs in most wells, pseudo sonic logs are generated wherever necessary using resistivity log data. Wells with available sonic logs are used to obtain a generalized relationship between travel time and resistivity and the relation is used within other wells to obtain pseudo sonic logs (Rudman et al. 1976). These are combined with density log data to generate impedance logs. Impedance logs in turn provide the reflection coefficients which are then convolved with a selected seismic wavelet (extracted from the actual seismic data) to obtain synthetic seismic trace. The synthetic traces are compared with the actual seismic traces observed from within a volume around the well track (mean computed over a cylindrical volume with 8 nearest traces) and major reflectors are matched to get acceptable ties (process is repeated for all available wells).

The modified seismic volume and logs obtained are used to predict reservoir wide log properties such as porosity and density maps using an ANN based approach. Seismic attributes (Chopra and Marfurt 2007) are calculated

from the actual seismic data and these attributes are used as inputs in a supervised ANN modeling framework which tries to match for the desired property as the output. These properties are useful inputs in the fracture characterization workflow and they also help in evaluating geomechanical properties using phase velocities. Impedance is then used to predict rock properties (ϕ, ρ, etc.) using data along well tracks for supervised ANN training and prediction. Relative acoustic impedance is independently computed using colored inversion workflow where a single inversion operator is derived that optimally inverts the data and honors available well data in a global sense. Since this requires sonic travel time data, only two control wells (with available sonic logs) are used in the inversion scheme. Pseudo logs from properties estimated using ANN based modeling are compared with actual logs to validate the property estimates before their use in characterization workflows if required.

Data integration and analysis

Next, we use SGEMS to populate the entire study volume by making use of COSGSIM algorithm involving seismic derived relative acoustic impedance as the secondary hard data. The choice of algorithm is based on its ability to reduce local uncertainty and improve resolution with adequate weight given to known structural features of the reservoir. Since the inputs need to conform to Gaussian distribution, normal score transformation is used to transform the input random function to a standard Gaussian distribution (Goovaerts 1997). Simulation uncertainty is computed based on normalized standard deviations observed at each evaluation point. The final selection of V_P and V_S model for further analysis and calculations is based on least square error evaluation using the original (sparse) velocity fields. **Figure 5** shows V_P and V_S realizations and final selected model at two randomly selected locations (Inline/ Crossline co-ordinates) for reference.

V_P and V_S can be related to elastic rock properties including bulk modulus, shear modulus and Poisson's ratio and these properties can be used to characterize zones of interest using available frameworks to relate the geophysical and geomechanical properties with reservoir attributes such as fractures (Toksoz and Johnston 1981). We know that compressional and shear velocities can be used to derive Lame's parameters using density data (Eq. 1 and Eq. 2). The Lame's parameters are in turn used to estimate the inertial properties of the rock using standard equations of elastic moduli (Eq. 3, Eq. 4 and Eq. 5).

$$\mu = \rho {V_S}^2 \quad (1)$$

$$\lambda = {V_P}^2 \rho - 2\mu \quad (2)$$

$$K = \lambda + 2\mu/3 \quad (3)$$

$$E = 9K\lambda/(3K + \mu) \quad (4)$$

$$\nu = \lambda/2(\lambda + \mu) \quad (5)$$

We can further calculate estimates of extensional and hydrostatic stresses directly using V_P and V_S estimates obtained earlier (Toksoz and Johnston 1981) as shown in Eq. 6 and Eq. 7.

$${\sigma_E}^2 = V_S^2(3V_P^2 - 4V_S^2)/(V_P^2 - V_S^2) \quad (6)$$

$${\sigma_H}^2 = {V_P}^2 - (1.33){V_S}^2 \quad (7)$$

Considering Hudson's fracture model using effective medium theory (Hudson 1990) and HTI anisotropy, weakness estimates (Hsu and Schoenberg 1993) can be measured based on selected fracture density "e" value. In this study, a sparse fracture density map based on image logs was used to estimate values over entire study volume under consideration. However, fracture density from other independent sources such as shear wave analysis or from prestack seismic data can also be used if available. Normal and tangential weaknesses can therefore be estimated as shared in Eq. 8 and Eq. 9.

$$\Delta_N = 4e/\{3(V_S/V_P)^2 \times [1 - (V_S/V_P)^2]\} \quad (8)$$

$$\Delta_T = 16e/\{3 \times [3 - 2(V_S/V_P)^2]\} \quad (9)$$

Extensional stress is known to have a direct bearing on fracture opening (Toksoz and Johnston 1981) while tangential weakness provides an estimate of fracture density (Downton and Roure 2010). While indicative in nature, more robust relationships can be developed and used for fracture properties based on core analysis. As an ex-

ample, Rutqvist showed that fracture aperture can be calculated from effective normal stress (Rutqvist and Tsang 2003) which we have modified to define the normalized fracture aperture expandability (Eq. 10).

$$F_E = (b - b_r)/b_{max} = e^{\alpha\sigma_E} \quad (10)$$

Where b_r, b_{max} and α parameters are obtained from laboratory and field measurements using empirical relations involving rock classification index. There are a number of observations which can be made using many of the estimated property maps, particularly by combining with properties estimated from seismic attributes. Apart from stress and weakness estimates, we also know that closing of small fractures due to increasing pressure with depth or cementation effects should cause an observed increase in seismic velocity. However, increased fracturing, chemical alteration and extreme temperature gradients, etc. can cause a reduction in seismic velocities. Fluid saturation tends to reduce V_S and enhance V_P/V_S ratio as well as Poisson's ratio. For highly fractured zones we can generally expect low V_P and V_S values as well as reduced compressional to shear velocity ratios. These and other effects such as effect of fractures on porosities, acoustic impedance, bulk densities, etc., can be used within an integrated characterization framework to identify fractured zones within the study area. **Figure 6** and **Figure 7** show sample maps for these derived properties at the reference depth of 0.5 km.

Fractured zone identification and characterization

The reservoir property estimates obtained from microseismic data analysis as well as those obtained from 3D seismic data using ANN – well log property prediction workflow can be combined based on the expected behavior of said properties within fracture zones. These include relatively high estimated porosities, lower densities and low impedance values. In addition, due to velocity attenuation effects, low V_P/V_S ratio anomalies and low V_P anomalies could be fracture induced. Similarly, low extensional stress anomalies can possibly indicate zones with open fractures (Hutchings et al. 2001 and Martakis et al. 2006). Each of these individual properties by themselves may not be indicative of fracturing with high degree of certainty due to similar observations under different reservoir conditions. As an example, while low V_P anomalies could be fracture induced, it could also be indicative of gas bearing formations. Therefore, a holistic look is necessary to map the fractured intervals based on the property perturbations in the study area. This is accomplished by combining the individual property maps into newly devised FZI attributes. While there could be many ways of designing such an attribute (based on which properties are defined as ANN nodal inputs), we use a simple relationship as defined in Eq. 11 for this study.

$$FZI = f(\phi_n, \rho_n, f_n, Z_n, V_{Sn}, V_{Pn}, \sigma_{En}, \Delta_{Tn}) \quad (11)$$

The FZI modeling for this study is performed using a simple multiplayer RBF algorithm where the activation functions used in the network are radial basis functions. **Figure 8** shows sample training data used for network training before application of the trained models on the entire study volume. Based on the available fracture logs, some locations are used for the training process while the others help in validation of the designed ANN model. Fracture opening can be mapped in a similar fashion as demonstrated with Eq. 12.

$$FZI_A = f(\phi_n, f_n, Z_n, F_E) \quad (12)$$

Fracture permeability can be estimated empirically based on Darcy flow using fracture density estimate (fractures per unit length) and fracture aperture estimate. However, since fracture density is unknown in absolute terms, we use mapped FZI probability to estimate fracture density by preselecting “minimum” and “maximum” fracture density values based on analysis of available image logs and generating scaled fracture density values for the entire study volume. Since we only have normalized fracture aperture estimates (FZI_A), fracture density map is also normalized. The following equation (Eq. 13) is used for fracture permeability estimation:

$$k_{Fi} = e_n {FZI_A}^3/12 \quad (13)$$

Where the normalized fracture density estimate is computed using the predefined densities as mentioned earlier. **Figure 9** shows sample FZI and k_{Fin} maps at reference depth of 0.5 km. All of the defined properties can be used in an integrated approach to characterize fracture dominated zones and better understand reservoir communication and well performance. However, before mapping the properties and making interpretations, zones showing very high uncertainties are trimmed out of these maps based on simulation and inversion uncertainties. The process of defining the cumulative uncertainty estimate is based on the model inputs being used for FZI property calculations. The velocity estimate uncertainties are evaluated using the estimated inversion error (e_i) as well as the simulation error (u_{VPs} and u_{VSs}) evaluated based on normalized model standard deviation as shared in Eq. 14a and Eq. 14b for V_P and V_S respectively.

$$u_{VP} = e_i u_{VPs} \quad (14a)$$

$$u_{VS} = e_i u_{VSs} \quad (14b)$$

Based on the evaluated velocity model errors, we can compute property estimate errors based on the rock physics models originally used in their evaluation. Despite significant errors in seismic derived properties, they are assumed to have insignificant estimation errors in order to simplify uncertainty evaluation. The following relations (Eq. 15, Eq. 16 and Eq. 17) provide the estimated errors for extensional stress and tangential weakness values:

$$u_{\sigma E} = u_{VS}^2(3u_{VP}^2 - 4u_{VS}^2)/(u_{VP}^2 - u_{VS}^2) \quad (15)$$

$$u_{\Delta T} = u_{VP}^2/u_{VS}^2 \quad (16)$$

$$u_{FZI} = w_{VP}u_{VP} + w_{VS}u_{VS} + w_{\sigma E}u_{\sigma E} + w_{\Delta T}u_{\Delta T} \quad (17)$$

Figure 10 shows the normalized inversion and simulation uncertainty maps as well as normalized uncertainty for the modeled FZI property for the same reference depth of 0.5 km. These uncertainty values are used to quality any qualitative or quantitative interpretations that may be made based on the final fracture attributes. **Figure 11** shows potential flow behavior near well locations at depths of 0.5 km and 1.0 km based on observed discontinuities and FZI attribute behavior. This method can be used to identify the zones of interest, either horizons within existing wellbores or new areas of interest within the study volume. Moreover, the identified fracture properties, though only indicative in nature, can provide estimates for inputs to fracture modeling and flow simulation workflows as deemed necessary.

Summary

Our work successfully demonstrates the possibility of using microseismic data to evaluate geomechanical properties which can provide a framework for fracture zone identification and characterization when combined with other information. This method can be applied under most unconventional reservoir settings (which incorporate passive seismic monitoring and have had atleast one baseline seismic survey) and allows use of microseismic data for characterization purposes (and not just injection monitoring). While we have developed a framework for fracture zone identification, the method can easily be used for other characterization workflows including for lithology, fluid type, fracture orientations, etc. Moreover, additional information such as injection/ production data and geologic models can also be integrated within the workflow to add additional constraints into the modelling process. Finally, this method also provides a framework for time lapse fracture characterization within the field by making use of temporally segmented catalogs of microseismic data.

Acknowledgements

This work was supported by Ormat Inc. and we acknowledge Ezra Zemach, Skip Matlick and Patrick Walsh from Ormat for providing us with the datasets to work with and for providing valuable guidance as and when requested. We used dGB's OpendTect software in this study and thank them for providing requisite student licenses to USC. We have used Matlab extensively including implementation of ANN modeling and would like to acknowledge Mathworks for providing required licenses.

Nomenclature

ANN = Artificial Neural Network
COSGSIM = Sequential Gaussian Co-Simulation
E = Young's modulus, m/Lt^2, kg/ms^2
F_E = normalized fracture expandability parameter
FZI = Fracture Zone Identifier
FZI_A = Fracture Zone Identifier - Aperture
HTI = Horizontal Transverse Isotropy
K = bulk modulus, m/Lt^2, kg/ms^2
LVQ = Linear Vector Quantizer
MEQ = Micro Earthquake
RBF = Radial Basis Function
SCEC = Southern California Earthquake Center
SGEMS = Stanford Geostatistical Modeling Software
V_P = compressional velocity, L/t, m/s
V_{Pn} = normalized compressional velocity
V_S = shear velocity, L/t, m/s

V_{Sn} = normalized shear velocity
V_{sh} = volumetric fraction of shale
Z_n = normalized impedance
b = aperture, L, μm
b_r = residual aperture, L, μm
b_{max} = maximum aperture, L, μm
e = fracture density, n/L^3, m^{-3}
e_i = inversion error
e_n = normalized fracture density
f_n = normalized frequency
k_{Fi} = fracture permeability
u_{FZI} = uncertainty in FZI estimate
u_{VP} = overall uncertainty for V_P
u_{VPs} = simulation uncertainty for V_P
u_{VS} = overall uncertainty for V_S
u_{VSs} = simulation uncertainty for V_S
$u_{\Delta T}$ = uncertainty in tangential weakness estimate
$u_{\sigma E}$ = uncertainty in extensional stress estimate
w_{VP} = trained ANN nodal weight for V_P node
w_{VS} = trained ANN nodal weight for V_S node
$w_{\sigma E}$ = trained ANN nodal weight for σ_E node
α = aperture calculation parameter (constant)
λ = Lame's parameter
μ = Lame's parameter
v = Poisson's Ratio
ϕ_n = normalized porosity
ρ = density, m/L^3, kg/m^3
ρ_n = normalized density
σ_E = extensional stress, m/Lt^2, kg/ms^2
σ_{En} = normalized extensional stress
σ_H = hydrostatic stress, m/Lt^2, kg/ms^2
Δ_N = normal weakness
Δ_T = tangential weakness
Δ_{Tn} = normalized tangential weakness

References

1. Aminzadeh, F., Maity, D., Tafti, T. and Brower, F. 2011. Artificial Neural Network based Autopicker for Micro Earthquake Data. Expanded Abstracts, SEG Annual International Meeting, San Anotnio, TX, USA, 1623-1626.
2. Bakker, P., Vanvliet, L.J. and Verbeek, P.W. 1999. Edge Preserving Orientation Adaptive Filtering. Proc., IEEE Int. Conf. Computer Vision, Pattern Recognition, Fort Collins, CO, USA, Vol. 1, 535-540.
3. Beer, F.P., Johnston, E.R., Dewolf, J. et al. 2009. *Mechanics of materials*. Singapore: McGraw Hill. ISBN: 0073380288.
4. Chopra, S. and Marfurt., K.J. 2007. Seismic Attributes for Prospect Identification and Reservoir Characterization. SEG. ISBN: 1560801417.
5. Downton, J. and Roure, B. 2010. Azimuthal simultaneous elastic inversion for fracture detection. Expanded Abstracts, SEG Annual International Meeting, Denver CO, USA, 263-267.
6. Faust, L.Y. 1953. A Velocity Function Including Lithologic Variation. *Geophysics* **18** (2): 271-288. http://dx.doi.org/10.1190/1.1437869.
7. Goovaerts, P. 1997. Geostatistics for Natural Resources Evaluation. Oxford University Press. ISBN: 0195115384.
8. Hsu, C.J. and Schoenberg, M. 1993. Elastic wave through a simulated fractured medium. *Geophysics* **58** (7): 964-977. http://dx.doi.org/10.1190/1.1443487.
9. Hudson, J.A. 1990. Overall elastic properties of isotropic materials with arbitrary distribution of circular cracks. *Geophys J Int* **102** (2): 465-469. http://dx.doi.org/10.1111/j.1365-246X.1990.tb04478.x.
10. Hutchings, L., Wagoner, J. and Berge, P. 2001. Rock Physics Interpretation of P Wave, Q and Velocity Structure, Geology, Fluids and Fractures at the South East Portion of the Geysers Geothermal Reservoir. Transactions, GRC Annual Meeting, San Diego, CA, USA, 1-23.
11. Jahne, B. 1993. Digital Image Processing, Concepts, Algorithms and Scientific Applications. Berlin: Springer. ISBN: 3540592989.
12. Lancaster, S. and Whitcombe, D. 2000. Fast track coloured inversion. Expanded Abstracts, SEG Annual International Meeting, Calgary, Canada, 1298-1301.
13. Maity, D. and Aminzadeh, F. 2012. Framework for time lapse fracture characterization using seismic, microseismic & well log data. Expanded Abstracts, SEG Annual International Meeting, Las Vegas, NV, USA. 1-6.
14. Martakis, N., Kapotas, S. and Tselentis, G. 2006. Integrated Passive Seismic Acquisition and Methodology: Case Studies.

Geophys Prospect **54** (6): 829-847. http://dx.doi.org/10.1111/j.1365-2478.2006.00584.x.
15. Mavko, G., Mukherji, T. and Dvorkin, J. 2003. The Rock Physics Handbook. Cambridge University Press. ISBN: 9780511738876.
16. Rudman, A.J., Whaley, J.F., Blakely, R.F. et al. 1976. Transformation of resistivity to pseudo velocity logs. *AAPG Bull* **59**: 1151-1165.
17. Rutqvist, J. and Tsang, C. 2003. Analysis of thermal–hydrologic–mechanical behavior near an emplacement drift at Yucca Mountain. *J Contam Hydrol* **62-63**: 637-652. http://dx.doi.org/10.1016/S0169-7722(02)00184-5.
18. Thurber, C.H. 1993. Local Earthquake Tomography: Velocities and Vp/Vs – Theory. In *Seismic Tomography: Theory and practice*, ed. H.M. Iyer and K. Hirahara, 563-583: Chapman and Hall.
19. Toksoz, M.N. and Johnston, D.H. 1981. Seismic Wave Attenuation. SEG. ISBN: 0931830168.
20. Waldhauser, F. and Ellsworth, W.L. 2001. A double-difference earthquake location algorithm: Method and application to the northern Hayward fault. *Bull Seismol Soc Am* **90** (6), 1353-1368. . http://dx.doi.org/10.1785/0120000006.

Figures

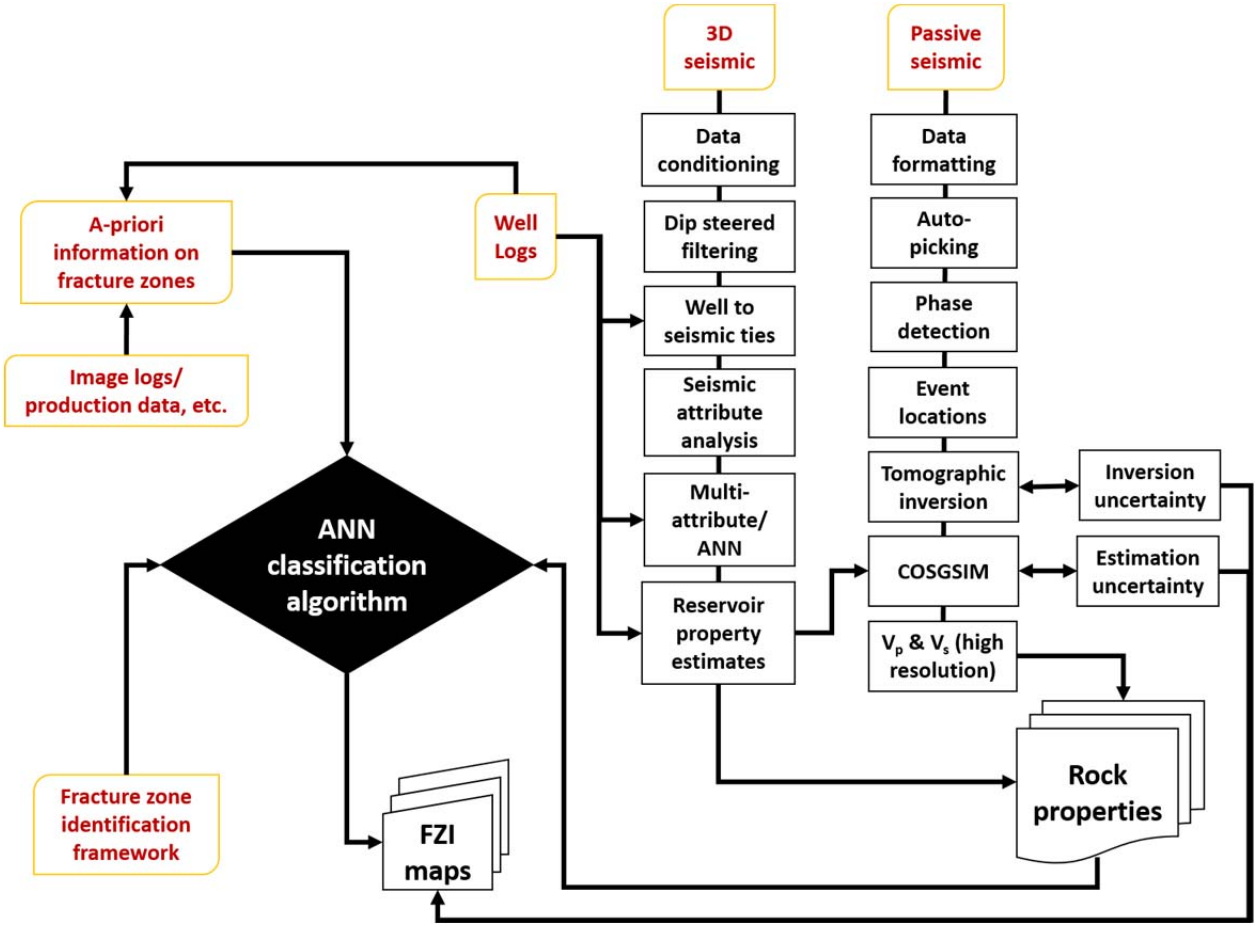

Figure 1: Fracture attribute (FZI) characterization workflow using 3D surface seismic, passive seismic and well log data

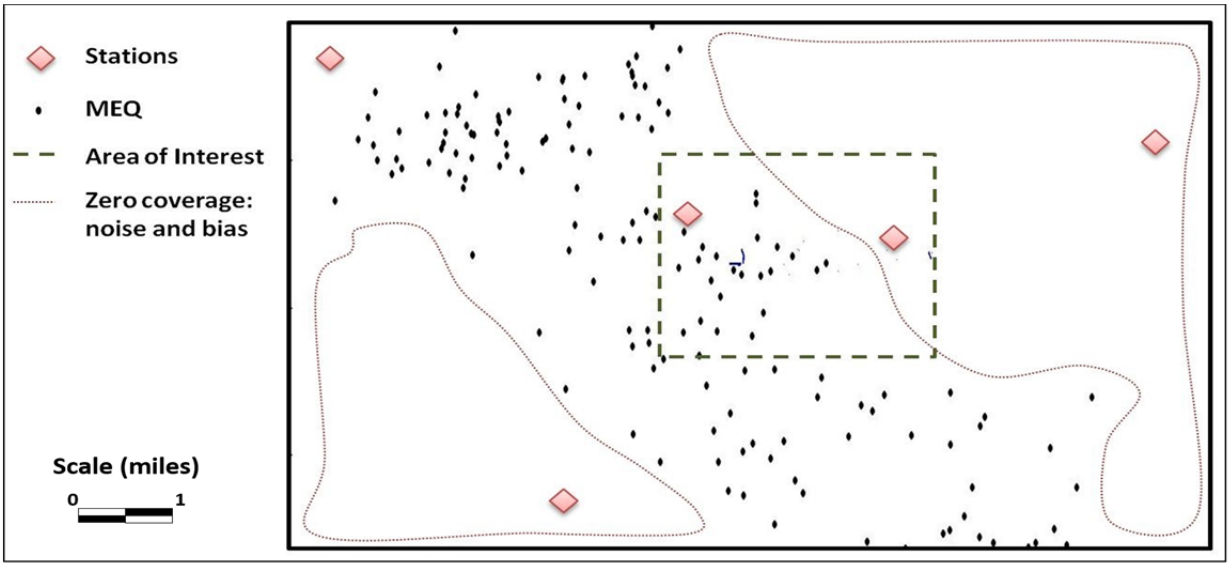

Figure 2: Spatial expanse of SimulPS 'finite node grid' with stations, events and study volume plotted for reference

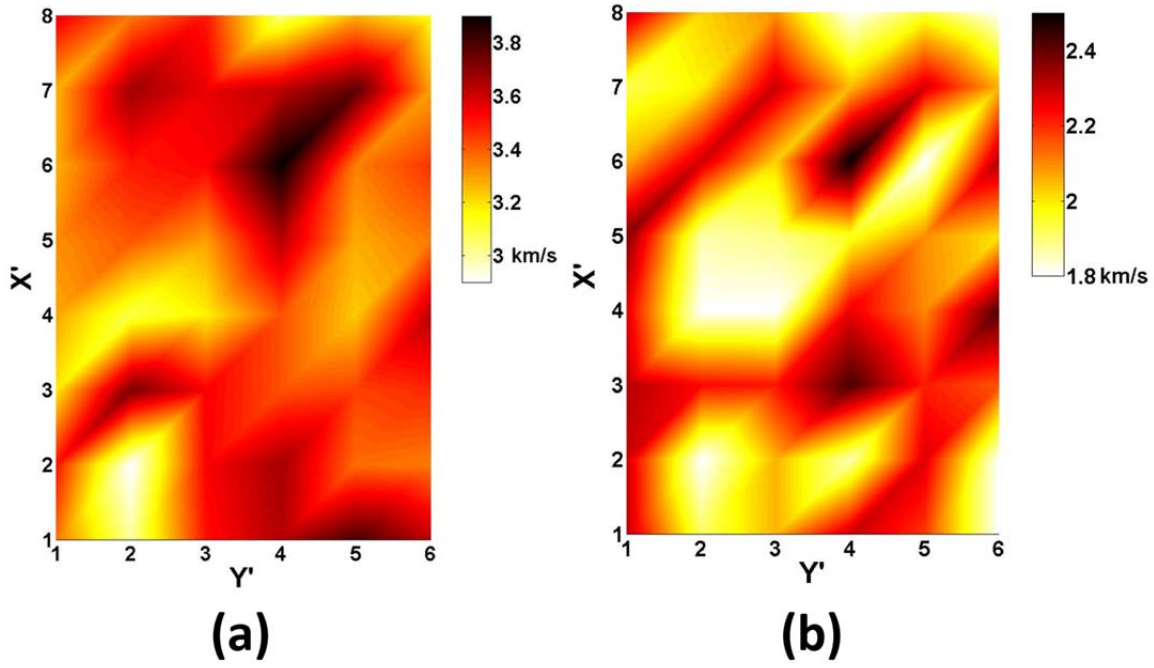

Figure 3: (a) V_P and (b) V_S maps from inversion (data range extracted from original velocity maps so as to conform to study volume dimensions)

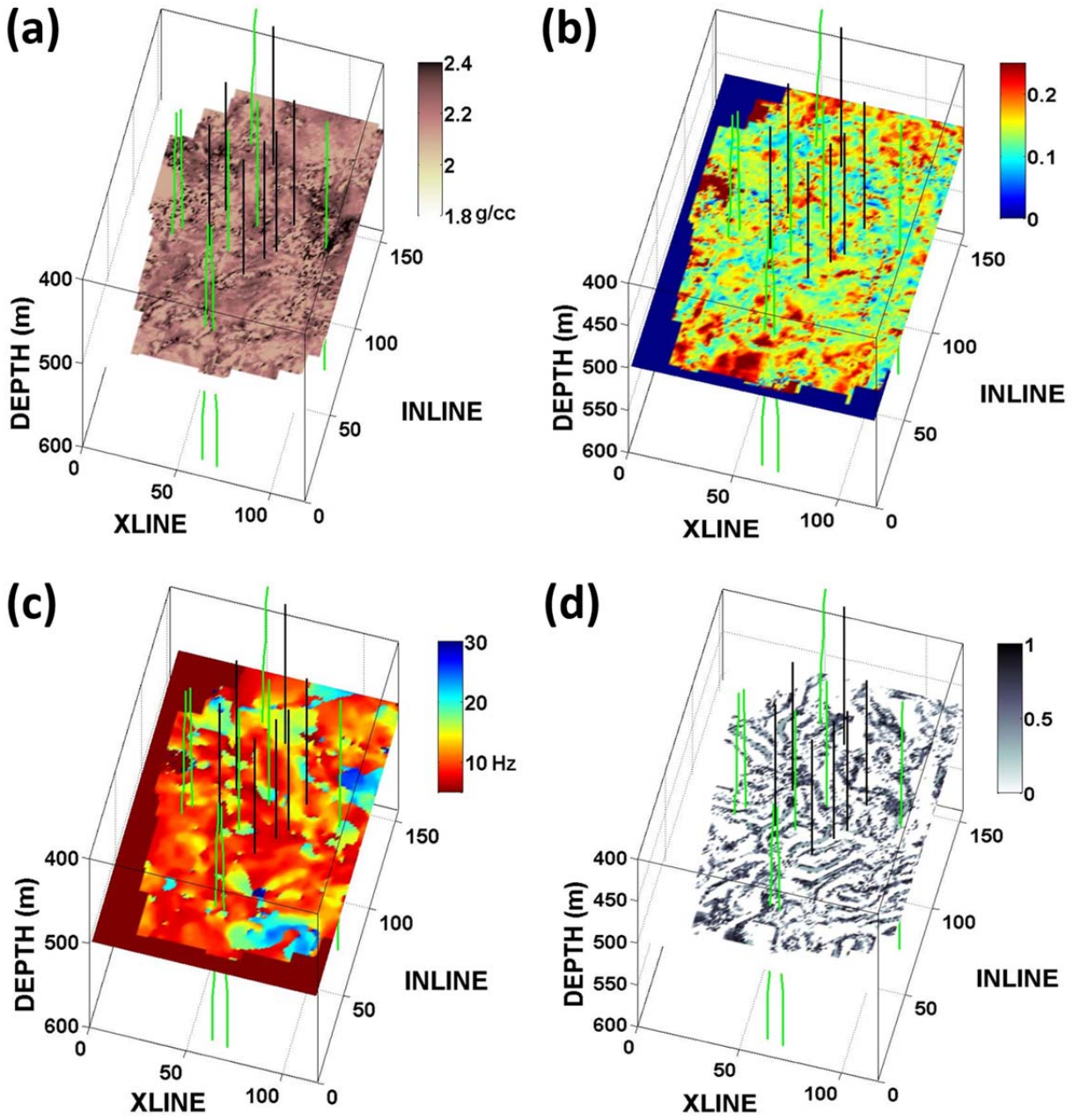

Figure 4 (a) Density, (b) Porosity, (c) Instantaneous frequency and (d) Discontinuity (ANN) map as observed at 0.5 km depth interval with injection (green) and production (black) well tracks

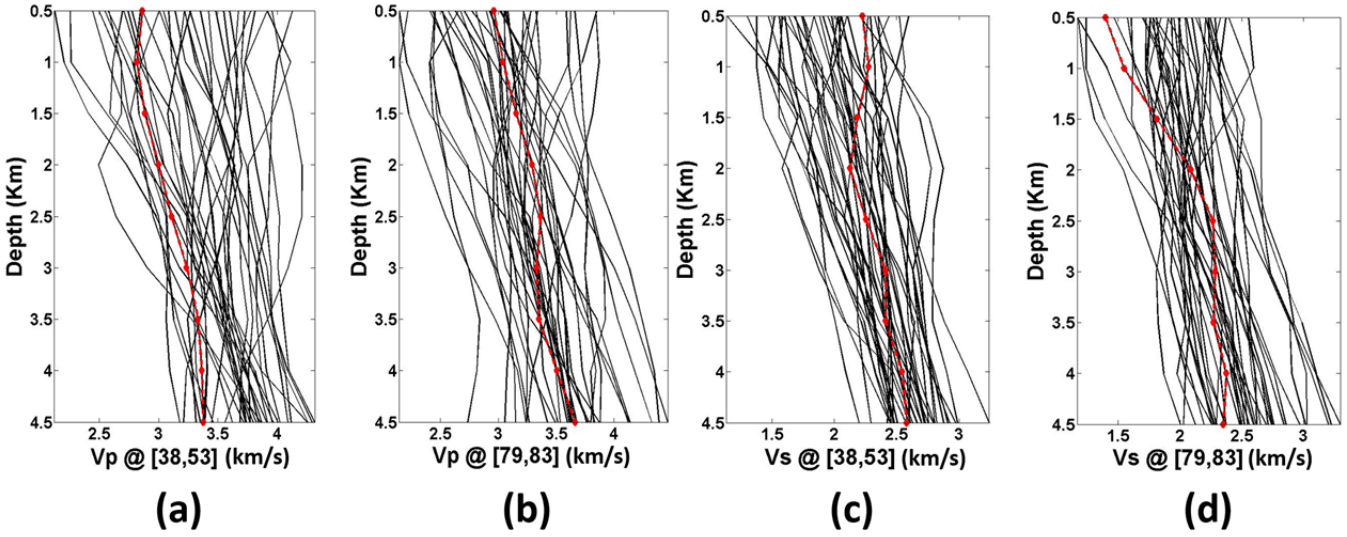

Figure 5: Subplots (a) and (b) show sample V_P realizations at two indexed locations and the final selected model (red) while subplots (c) and (d) show sample V_S realizations at the same selected locations including the final model (red)

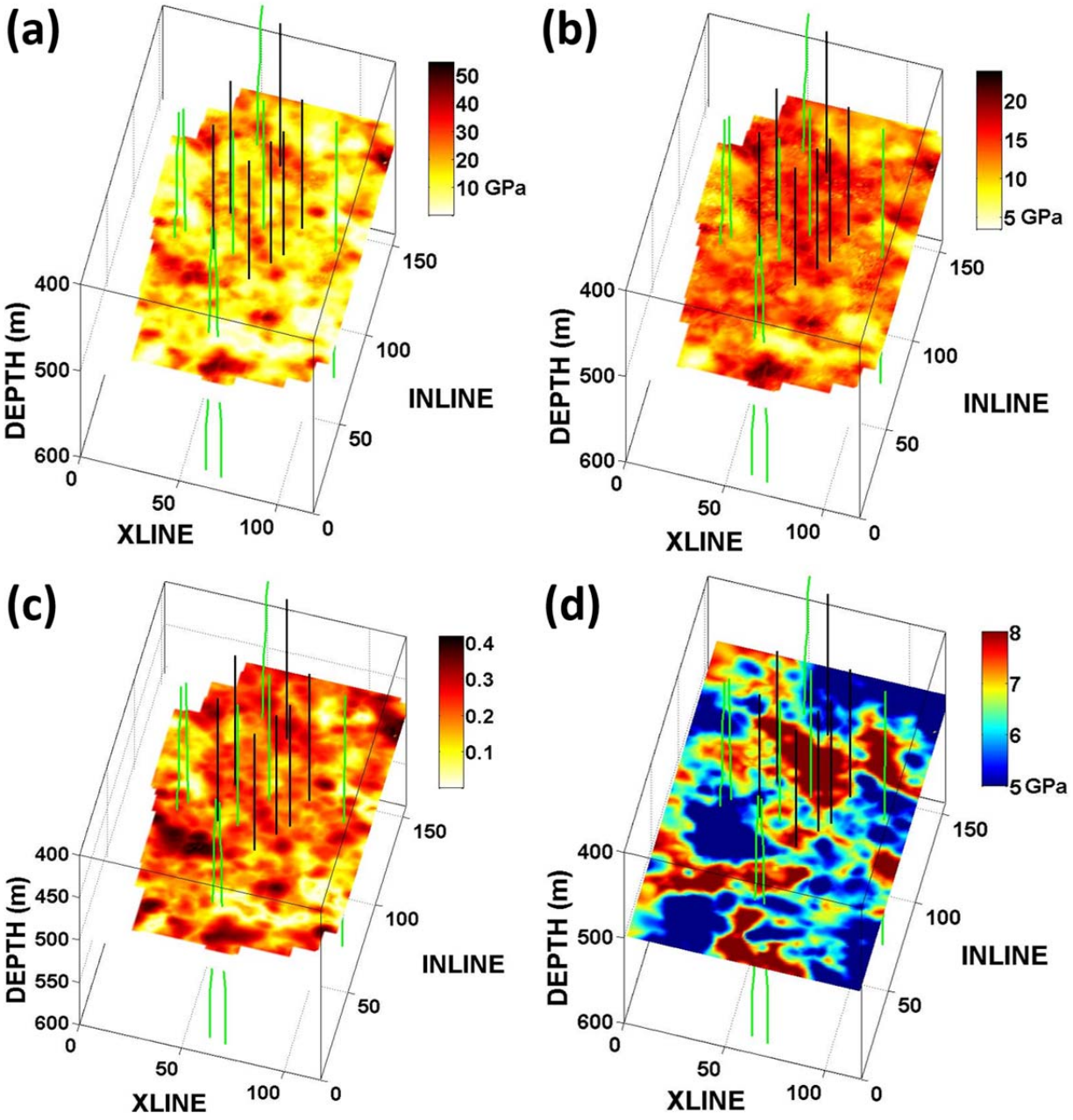

Figure 6: (a) Young's Modulus, (b) Bulk Modulus, (c) Poisson's Ratio and (d) Extensional stress mapped at reference depth of 0.5 km with injection (green) and production (black) well track inserts

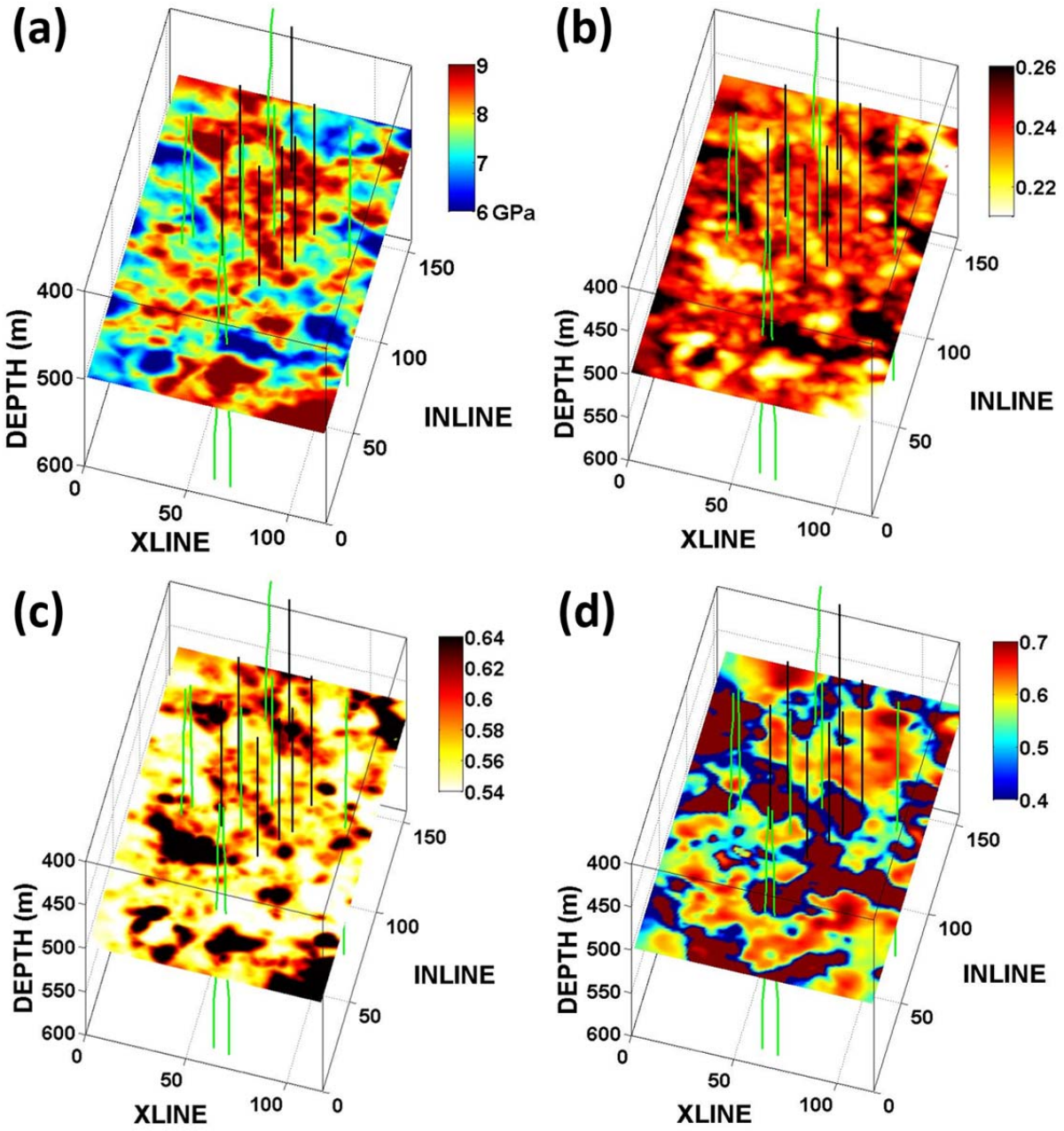

Figure 7 (a) Hydrostatic stress, (b) Tangential weakness, (c) Normal weakness and (d) Fracture aperture expandability mapped at reference depth of 0.5 km with injection (green) and production (black) well inserts

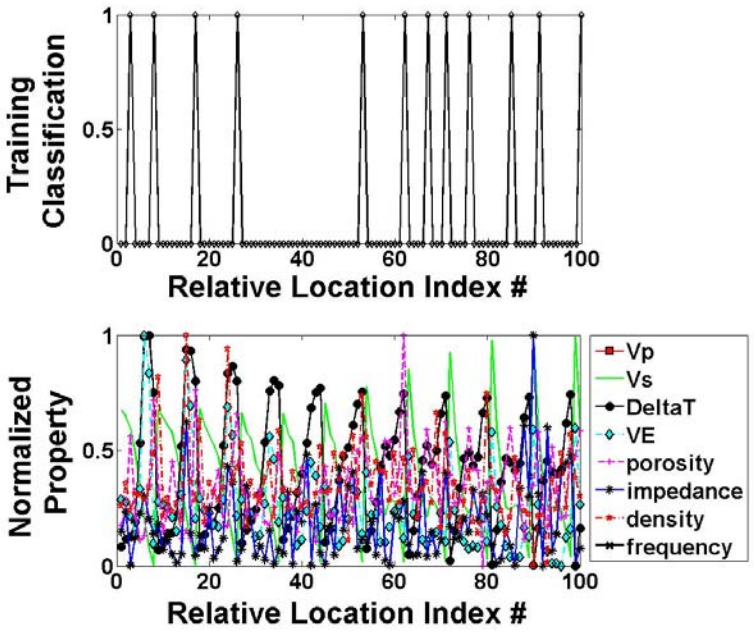

Figure 8: Sample training data and input properties used for derived FZI property mapping. The selected properties are normalized and used as inputs through ANN nodes

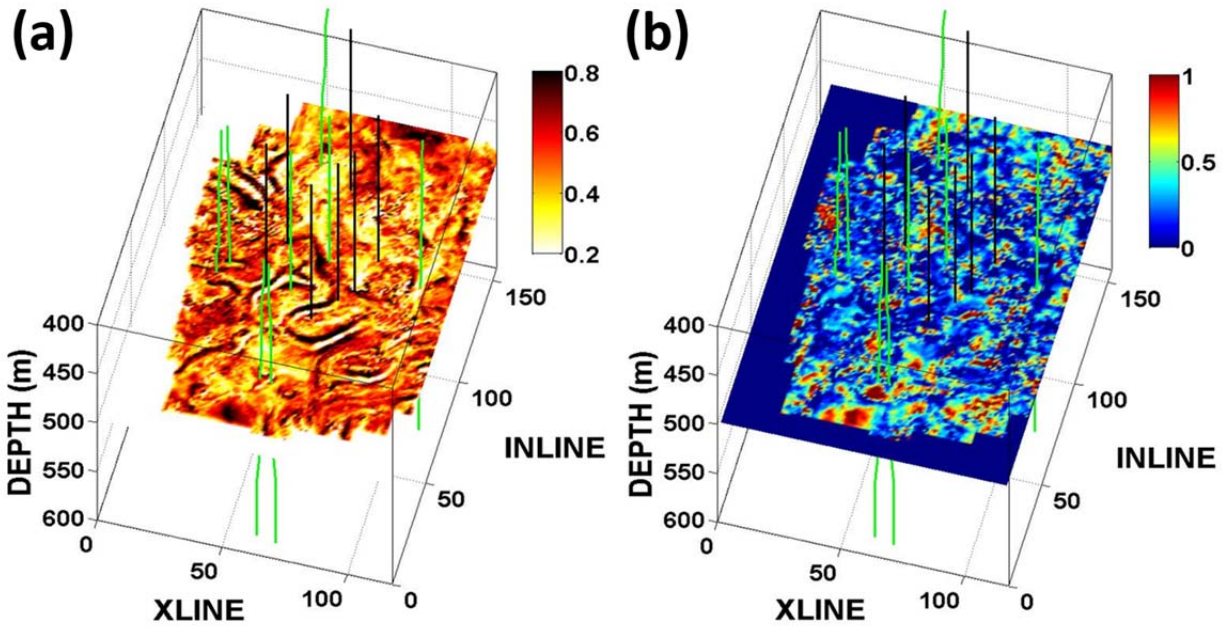

Figure 9: (a) FZI and (b) normalized k_{Fi} maps at reference depth of 0.5 km

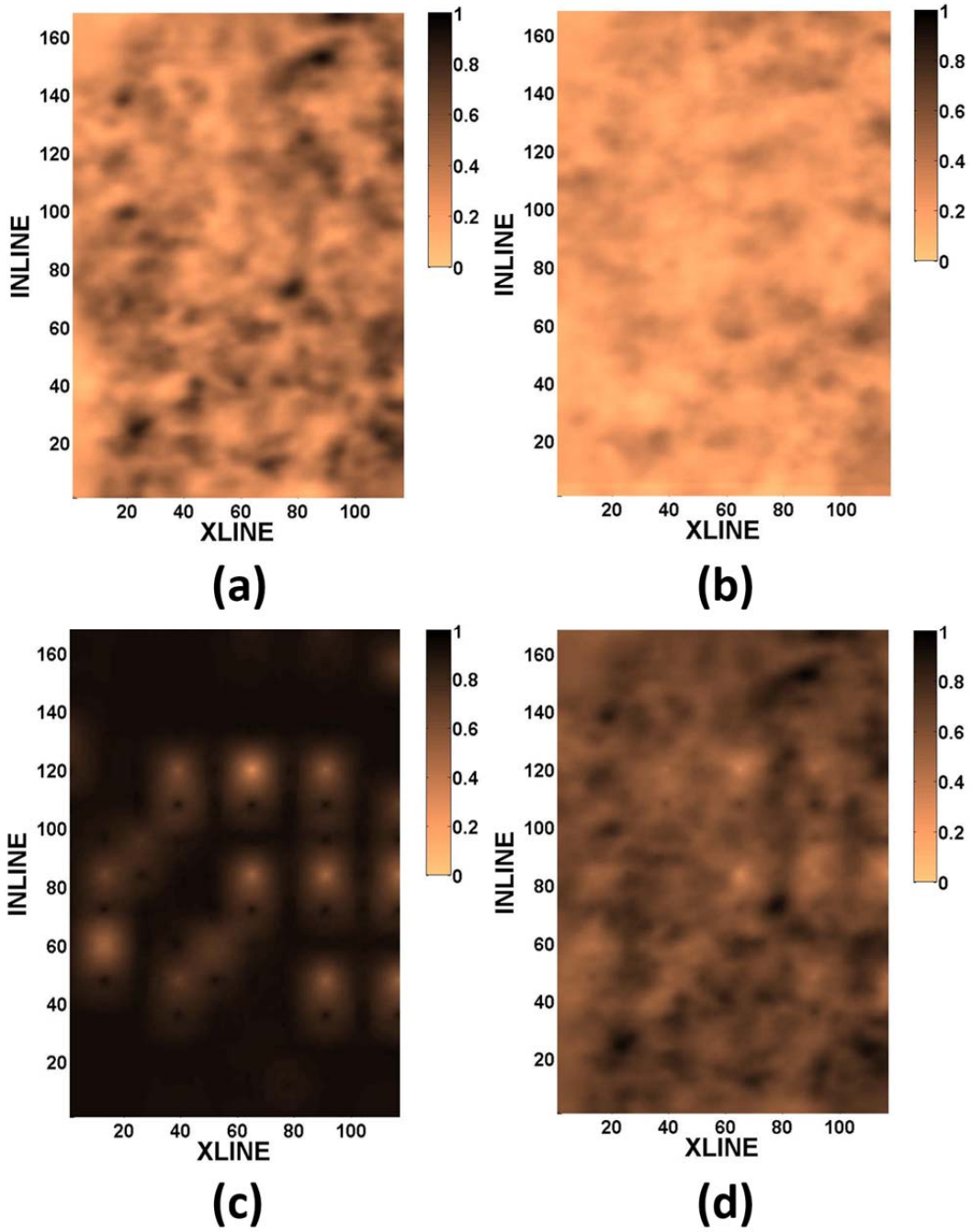

Figure 10: (a) V_P simulation uncertainty map, (b) V_S simulation uncertainty map, (c) inversion uncertainty map and (d) FZI uncertainty map at reference depth of 0.5 km

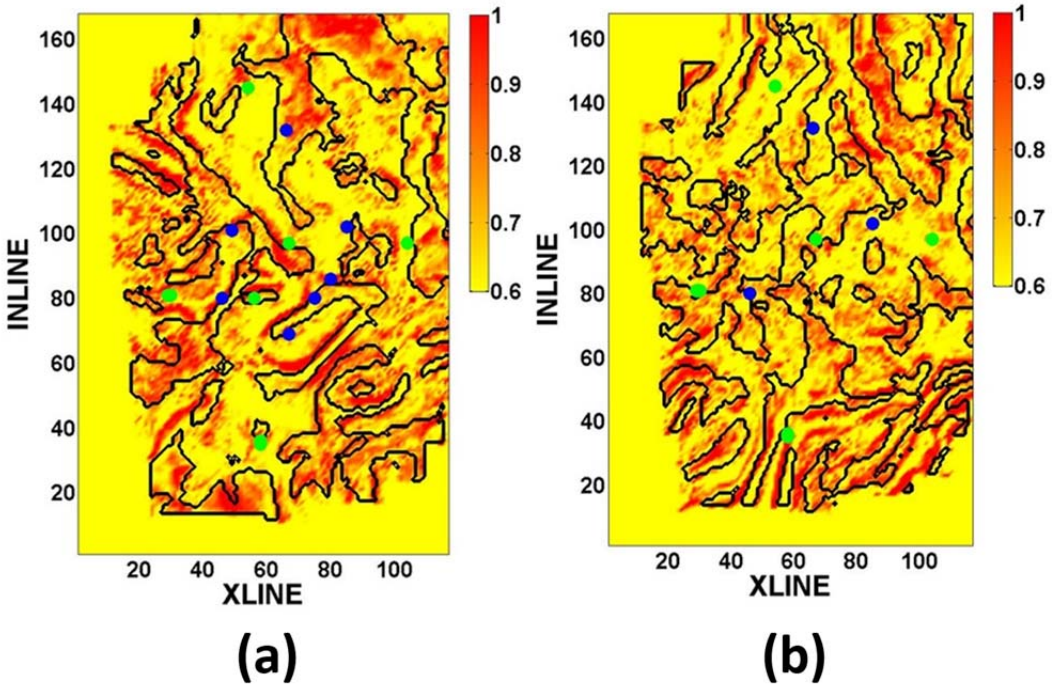

Figure 11: FZI with discontinuity derived from 3D seismic data used to identify and validate flow regimes close to known injectors (green inserts) and producers (blue inserts). Subplot (a) shows mapping at 0.5 km while (b) shows mapping at 1.0 km. Some wells align with major edge boundaries and/ or fall within high FZI zones.